Ocean Science
Discussions

Open Access

OSD

Interactive
comment

Interactive comment on "High-resolution diapycnal mixing map of the Alboran Sea thermocline from seismic reflection images" *by* Jhon F. Mojica et al.

Jhon F. Mojica et al.

jfm11@nyu.edu

Received and published: 1 November 2017

First, we want to thank referee#2 for her/his effort. We found the comments and suggestions very useful, and we have tried to answer and/or follow all of them as indicated in our point-by-point answers below. To clarify our answers, we add a file (Review2-answer1.pdf) as a supplement, easily to read for you.

Thanks for the comment. We first want to make clear that the goal of the paper is not presenting the details of the data processing and spectral analysis, nor developing a new method to estimate mixing. The method used to produce the diapycnal diffusivity map from seismic data is not new; it is analogous to that presented in previous works

(i.e. Sheen et al, 2009; Holbrook et al, 2013). In addition, the seismic data and their spectra were recently processed, analyzed and interpreted in detail in another paper by our group (Sallares et al. 2016). In fact, many of the questions raised by referee#2 are addressed in this paper. We have modified the text to make it clearer in the new version of the manuscript (line 100-102, 137-141). We would like to emphasize that our goal and original contribution of the paper are (1) producing a diapycnal mixing map of higher resolution than any previously existing one and (2) applying it for the first time to shallow waters (thermocline), a critical area to study mixing processes. We then try to interpret the observed features based on the results but also on our previous work. To do this, we use data acquired in the Alboran basin with high-resolution multichannel seismic system, which were presented, processed, analyzed and interpreted by Sallares et al. (2016). The basic points of the method applied to produce the maps are explained in this manuscript, and the details can be found in the other two works mentioned above. We clarify this in the new version of the manuscript (lines 186-189 rewritten).

The size of the window to calculate the spectra and to estimate the mixing values is always 1200 m wide x 15 m high. The difference with previous similar works is that the windows overlap with each other; The center of the window moves only 30 m in horizontal, and 3 m in vertical in each step. By doing this, the transition is smooth because we incorporate few new data in each new analyzed window. We can see the effect in figure rev2-1. (a) Mixing map obtained following a "conventional" way (i.e. no overlapping windows). In this case we apply a step of dx=1200 m, dz=6 m between 1200 m wide x 6 m high neighboring windows. (b) Mixing map obtained using 1200 m wide x 15 m high overlapping windows and a dx=30 m, dz=3 m step. The distribution and k(x,z) values is equivalent to (a) but display smoother transitions, making the map look more "realistic". This type of representation is new, but as we stated above, the method to estimate k(x,z) based on the horizontal wavenumber spectra of seismic reflectors is not new. We clarify all this in the new version of the manuscript (lines 197-199, 272-273, 298-300).

We cut the long tracks in 1200 m-long segments so that they fit inside the windows. This does not affect the spectrum at the spatial range analyzed. As an example, we analyze in figure rev2-2 a 16 km-long reflector (H3). We first calculate the spectrum for the whole reflector and we then split it in 10 segments (1.6 km each), and calculate their individual spectra as well as the average. The average spectra is very similar to the complete one in terms of energy and slope at the scale of interest. The details on the procedure followed to calculate the spectra can be found in Sallares et al. (2016) (line 193-194).

As we already explained above: (1) 30x3m is not the grid cell, it is just the step applied to analyze a new "1200 m-long x 15 m-high" window. (2) The size of the windows (so that of the actual grid cells) is always 1200x15m. (3) The tracks longer than 1200 m are cut into smaller segments that fit inside the window. Concerning resolution, we must distinguish between the theoretical resolution of the seismic data and that of the diapycnal mixing maps. For seismic data, the vertical resolution (i.e. the capability to discern between neighboring reflectors) is given by the Rayleigh criteria, whereas the horizontal resolution (i.e. the part of a reflector covered within half a wavelength of the seismic signal) corresponds to the first Fresnel zone. As we explain in Sallares et al. (2016), for our acquisition system, medium properties, and target depth, these are 1-2 m and 12-15 m, respectively. However, this does not represent the resolution of the mixing map. In this case, we are calculating spectra and diapycnal mixing within windows of 1200x15 m, so this could be taken as the approximate resolution of the map (in fact resolution is higher thanks to the "sliding window" approach). In summary, we do not claim that we are resolving structures of 30x3m, but the clear, larger-scale yellowish patches of 1-3 km-wide x 10-20 m-thick that are clearly identified in the map (better explained now in lines 209-212).

As we explained above, our study builds on previous work concerning both method and data. The method to produce diapycnal mixing maps based on horizontal wavenumber spectra of seismic reflectors is described in Sheen et al. (2009) and Holbrook et al.

C3

(2013). The data, including acquisition system, MCS data processing, reflector track-ing, S/N estimation, spectral analysis and statistical analysis of the obtained spectra, are presented in detail in Sallares et al. (2016) (in the main documents and supplemen-tary material). We do not think that it is necessary to repeat what is already explained and shown in these papers, but we could add part of it as supplementary material if the referee and editor think otherwise (e.g. figs. Rev2-3 or 2-4). In any case, we have introduced several changes in the text to clarify this (line 100-101, 186-189).

As we explained above, the original data, including the 68 reflectors and the criteria to select and track them, are shown and described in Sallares et al (2016). As you can see in figure rev2-3, they are rather homogeneously distributed throughout the analyzed area (30-110 m depth), so most of the 1200x15m analyzing windows contain reflectors and contribute to create the map. The few that do not have enough data to calculate the spectra are shown in white. We clarify this in lines 137-141.

At this sub-mesoscale ($\sim$window size) we apply the Gregg89 approach (Gregg, 1989), which considers the Garret-Munk model (Garret and Munk, 1979). The observations agree with the model predictions sufficiently well to assume that it describes the link between internal waves and turbulence. The interpretation is that the model is close enough to reality to capture the principal interactions scaling the turbulent dissipation in the thermocline (line 162-165).

Several single-track spectra, as well as the combined spectra of all reflectors for two different seismic profiles including the one analyzed here, are presented in detail in Sallares et al (2016). Both the single and the combined spectra (fig rev2-4) consis-tently show analogous spectral slopes and slope breaks at the same horizontal scales. Additionally, the spectral slopes coincide with theoretical estimations for three different, well-known sub-regimes: the Garret-Munk model for internal waves at >100 m, Kelvin-Helmholtz instabilities at $\sim$100-30 m, and Batchelor model for turbulent regimes (< 30 m) (line 137-141, 150-152).

C4

This issue is also addressed in Sallares et al (2016). As it can be observed in fig rev2-4, the combined spectra of the 68 spectra show clear slope changes consistent with theoretical estimates for the three sub-regimes referred to above at precise wavenumbers ($\sim$100 m and $\sim$30 m, respectively). The bound between the IW and shear instability regimes coincides with lN=$2\pi\Delta$V/N, where N is the buoyancy frequency, and ΔV is the root mean square amplitude of the velocity fluctuation about the mean, which is also calculated within the targeted depth range (30-110 m) from ADCP data. The same spectral slopes and bounds are also obtained in the other seismic profile analyzed in Sallares et al (2016). This behavior also holds for most of the individual tracks. Note that otherwise we would not obtain such clear trends in the combined spectra (fig rev2-4) (137-141, 152-156). Our interpretation in Sallares et al. (2016) is that the energy cascade between internal waves and turbulence at the sheared thermocline presents a distinct transitional subrange, possibly governed by vortex sheet dynamics. We suggest that the transition starts with the inset of shear instability along the stratified thermocline, follows with the development and rollup of KH billows, and ends with their breaking, collapse and dissipation. The energy needed to maintain these spectra comes from internal waves generated by tidal forcing at the Gibraltar strait, which are in turn subjected to a constant shear between the Atlantic and Mediterranean waters. Even though our analysis is local, the fact that the individual spectra display systematically the same transitional subrange at about the same scales, strongly suggests that this chain of processes is occurring continuously and simultaneous over the whole surveyed area (lines 150-152).

We do not refer to all sub-mesoscale structures "in general", but just to the internal waves that affect this region. The variations in diapycnal diffusivity show no clear correspondence with internal waves, but rather with the shear instability-like features identified in the transitional range between 100-30m (figures 7-8). We have modified the text to clarify this (line 19-21, 248-250, 339-341).

Thanks for the recommendation. We do agree and, in fact, we already examined the

Interactive comment

Printer-friendly version

Discussion paper

turbulent subrange to check if there was any correspondence between the features observed in this subrange (<30 m) and in the other two, and with the location of "mixing hotspots". We show two examples for H1 and H2 in figures rev2-5 and 2-6, respectively. It appears that it could be (fig rev2-5d), but the problem is that this subrange is too close to the resolution limit, especially in the vertical dimension of the analyzed structures, so data are rather noisy and it does not allow extracting meaningful conclusions.

Saying that the results agree "within uncertainty bounds" was an overstatement from our side. We have changed this in the new version. What we actually meant is that the global average and the values obtained with the XCTD are "within the range of values" obtained from the seismic data analysis (compare figs 4 and 5). We have reworded the text accordingly (line 22-24, 376-379).

Thanks for the comment. First, we agree that the relationship between IWs and over-turning is unclear and not directly justified by our results, so we have dropped this part from the text. Second, the relationship between shear instabilities and mixing hotspots comes from the analysis of various reflectors, not just H1 and H2. Here we show another reflector (H4) that show a similar pattern to H1. What we actually see is a correspondence between areas showing high diapycnal diffusivity and the location of the largest-amplitude features in the transitional domain, which we interpret to correspond to shear instabilities (possibly KH billows) based -also- on the results of Sallares et al. (2016). We have reworded lines 260-263 to clarify this.

The average k values presented in figure 4a is just a reference to compare with the range of values that we obtain from the seismic data. This way we confirm that our values are consistent with the ones inferred using more conventional oceanographic methods (same order of magnitude). But we fully agree that the main point of our results is the patchy nature and the range of variability (of over 4 orders of magnitude) in k. In this sense, we agree that the mean MCS/XCTD values shown in fig 4 were misleading so we have deleted them and we have incorporated instead a shadowed rectangle indicating the range of values obtained in the maps, which coincide with the

range of values obtained from the XCTD (new figure 4).

We agree that the hydrographic data are limited. However, these are the only "quasi-synoptical" data that we have, and we think that it is valuable to incorporate them in the discussion. The fact that both the average values for the whole column as well as the range of variability obtained from the XCTD compare well with those obtained from the –completely independent- seismic data is, in our opinion, a relevant result that is worth mentioning.

As it is explained in Sallares et al. (2016), an important step towards the calculation of the slope spectra is to suppress the random noise from the data and concentrate the analysis in the frequency bands where signal is clear. This can be efficiently done by: (1) estimating the signal-to-noise ratio (S/N) in the different frequency bands, and (2) selecting and applying a band-pass frequency filter that maximizes S/N. To estimate S/N we have applied a cross-correlation-based analysis that consists of the following steps:

i) Band-pass filtering the data;

ii) Calculate the cross-correlation (CC) between each seismic trace and all its neighbors within a distance equal to the length of the shortest reflectors used in the spectral analysis, dCC=1,250 m. This is first done in the upper part of the profile (30-120 m), hence the section that we consider to contain the signal.

iii) Calculate the maximum value of the CC within a time window corresponding to the mean separation between contiguous reflectors, tCC =10 ms, for each couple of traces (MaxSigij);

iv) Calculate the average value of MaxSigij for each seismic trace along the whole profile (AvMaxSigi);

v) Repeat steps ii) to iv) for the bottom part of the profile (120-240 m), which we consider to be noise, to obtain AvMaxNoisei;

Interactive comment

Printer-friendly version

Discussion paper

vi) Calculate the ratio $S/Ni=AvMaxSig_i/AvMaxNoise_i$ for each seismic trace;

vii) Calculate the average value of S/Ni for all the seismic traces: $< S/Ni>=S/N$;

viii) Repeat steps i) to vii) for the next frequency band.

No, we have not formally analyzed the statistical correlation between different signals. What we mean is that there is a visual correspondence between different features, as it happens, e.g., between high values of diapycnal mixing and large-amplitude features in the transitional domain. We have changed the word "correlation" by less confusing ones as "visual correspondence", or similar, in the new version of the manuscript (line 292, 336, 383).

We have modified the figure caption and text as suggested to briefly describe the procedure as follows: Figure 6 shows the average horizontal spectrum of the vertical displacement of tracked reflectors ($\Phi_\varsigma x$) scaled by the local buoyancy frequency at the reflector depth ($N/N0$) to eliminate stratification effects, and multiplied by $(2\pi kx)2$ to enhance slope variations (blackline). The reference lines are theoretical slopes of Garrett-Munk internal wave model [Garret and Munk, 1979] (red line), Kelvin-Helmholtz instabilities [Waite, 2011] (blue line), and Batchelor's model for turbulence [Batchelor, 1959] (green line).

Please also note the supplement to this comment:
https://www.ocean-sci-discuss.net/os-2017-72/os-2017-72-AC2-supplement.pdf

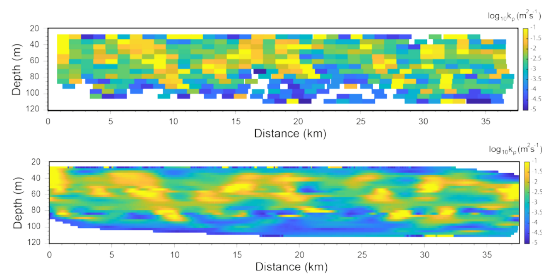Interactive comment on Ocean Sci. Discuss., https://doi.org/10.5194/os-2017-72, 2017.

Figure rev2-1. $k_p(x, z)$ map obtained along the seismic profile. (a) without sliding window, using window size (1200 x 6 m) just getting one point for each window move, (b) applying sliding window, using window size (1200 x 15m) with step (dx=30, dz=3m). The trends and values are equivalent, but (b) looks more continuous and, to us, more realistic.

Fig. 1.
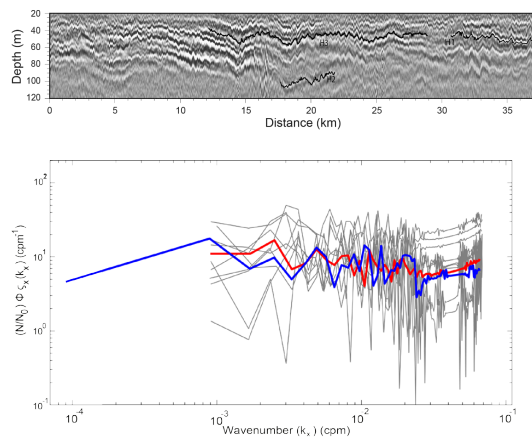
Figure rev2-2 (a) Depth-converted high-resolution multichannel seismic profile (Here we show a new horizon H3). (b) Horizontal spectrum of the vertical displacement of reflector H3. (blue line) considering the whole reflector. (gray lines) spectrum from the reflector split in ten 1.6 km-long segments. (red line) average spectrum from the 10 segments. The average of the 10 segments and the whole reflector show the same trends in the scales of interest.
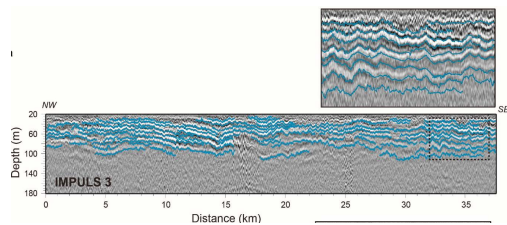
Fig. 2.

Figure rev2-3. Processed and depth-converted HR-MCS images along profile IMPULS-3, with
the tracked reflectors used in the spectral analysis superimposed (blue lines). The depth range of
the tracked reflectors is 30-100 m. The inset is a zoom over the area encompassed by the dashed
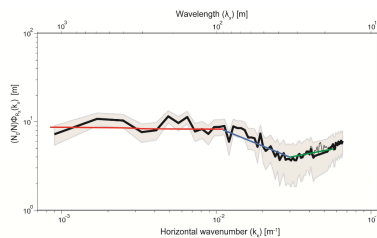rectangles (fig S5 in Sallares et al., 2016).

Fig. 3.

C11

Figure rev2-4. Average horizontal spectrum of the vertical displacement, scaled by the local buoyancy, obtained for the 68 reflectors (solid line) and their corresponding 95% confidence interval (2σ) (shaded area). The reference lines are the theoretical slopes corresponding to the GM79 model for the internal wave subrange (red line), Kelvin-Helmholtz instabilities for the transitional/buoyancy subrange (blue line), and Batchelor59 model for turbulence (green line). The dashed line follows the original, unfiltered part of the spectra in the region affected by harmonic noise arising from repeated shooting. This is eliminated by applying a stop band of 0.027 to 0.021 Hz.
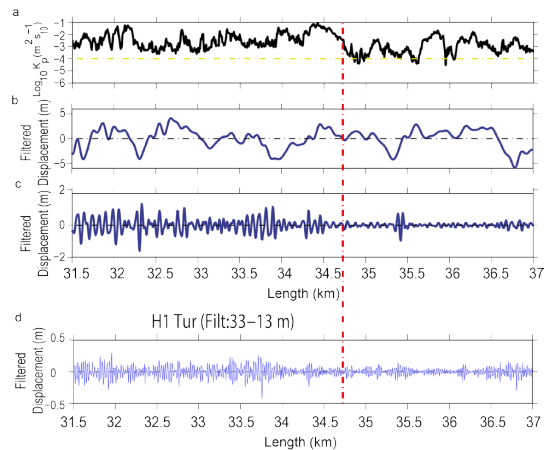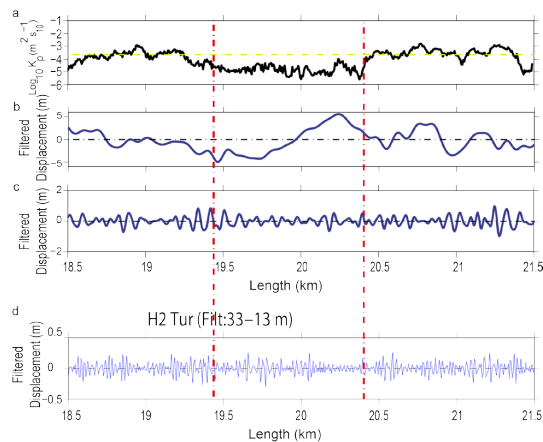
Fig. 4.

Figure rev2-5. (a) Diapycnal mixing obtained along H1 (see details of calculation in the text). (b) Signal filtered at wavelength ranges of the IW sub-range (*3000-100 m*), (c) the transitional subrange (*100-33 m*), (d) and the turbulence subrange (33-13 m). The dashed red line identifies the "breaking point" referred to in the text.

Fig. 5.

Figure rev2-6. (a) Diapycnal mixing obtained along H2 (see details of calculation in the text). (b) Signal filtered at wavelength ranges of the IW sub-range (*3000-100 m*), (c) the transitional subrange (*100-33 m*), (d) and the turbulence subrange (33-13 m). The dashed red line identifies the "breaking point" referred to in the text.
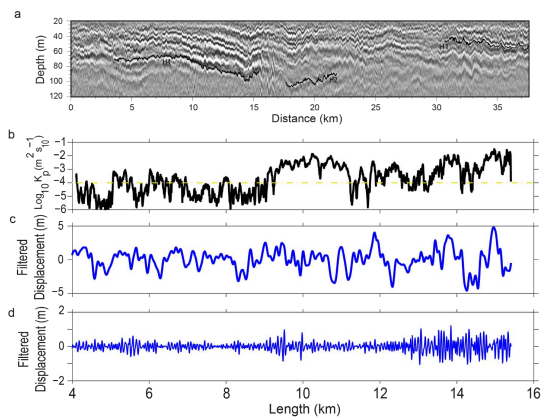
Fig. 6.

Figure rev2-7. (a) Location of H4 reflector. (b) Diapycnal mixing obtained along H4. (c) Signal filtered at wavelength ranges of the IW sub-range (*3000-100 m*), (d) the transitional subrange (*100-33 m*).

Fig. 7.